Materials Today Bio 28 (2024) 101165

Contents lists available at ScienceDirect

Materials Today Bio

journal homepage: www.journals.elsevier.com/materials-today-bio

Virucidal activity of porphyrin-based metal-organic frameworks against highly pathogenic coronaviruses and hepatitis C virus

Orfeas-Evangelos Plastiras [a,b], Peggy Bouquet [c], Imelda Raczkiewicz [b], Sandrine Belouzard [b], Esther Martin De Fourchambault [b], Jeremy Dhainaut [a], Jean-Philippe Dacquin [a], Anne Goffard [b,**], Christophe Volkringer [a,*]

[a] Unité de Catalyse et Chimie du Solide (UCCS), Univ. Lille, CNRS, Centrale Lille, Univ. Artois, F-59000, Lille, France
[b] U1019, UMR 9017, CIIL - Center for Infection and Immunity of Lille, Institut Pasteur de Lille, Université de Lille, CNRS, INSERM, CHU de Lille, 59000, Lille, France
[c] Clinical Microbiology Unit, Institut Pasteur de Lille, Lille, F-59000, France

ARTICLE INFO

Keywords:
Metal-organic framework
Antiviral
SARS-CoV-2
HCoV-229E
Hepatitis C virus

ABSTRACT

The antiviral effect of four porphyrin-based Metal-Organic Frameworks (PMOFs) with Al and Zr, namely Al-TCPP, PCN-222, PCN-223 and PCN-224 was assessed for the first time against HCoV-229E, two highly pathogenic coronaviruses (SARS-CoV-2 and MERS-CoV) and hepatitis C virus (HCV). Infection tests *in vitro* were done under dark or light exposure for different contact times, and it was found that 15 min of light exposure were enough to give antiviral properties to the materials, therefore inactivating HCoV-229E by 99.98 % and 99.96 % for Al-TCPP and PCN-222. Al-TCPP diminished the viral titer of SARS-CoV-2 greater than PCN-222 in the same duration of light exposure, having an effect of 99.95 % and 93.48 % respectively. Next, Al-TCPP was chosen as the best candidate possessing antiviral properties and was tested against MERS-CoV and HCV, showcasing a reduction of infectivity of 99.28 % and 98.15 % respectively for each virus. The mechanism of the antiviral activity of the four PMOFs was found to be the production of singlet oxygen $^1O_2$ from the porphyrin ligand TCPP when exposed to visible light, by using sodium azide (NaN_3) as a scavenger, that can later attack the phospholipids on the envelope of the viruses, thus preventing their entry into the cells.

1. Introduction

Coronaviruses, which belong to the family of *Coronaviridae* and subfamily of *Orthocoronavirinae*, are single-stranded RNA viruses having a length of 26–32 kilobases and consist of four genera: *Alphacoronavirus, Betacoronavirus, Gammacoronavirus* and *Deltacoronavirus*. HCoV-229E is one of the viruses that belongs to the genus *Alphacoronavirus* that causes mild symptoms of common cold in humans. The *Betacoronavirus* also known as Severe Acute Respiratory Syndrome Coronavirus-2 (SARS-CoV-2), is accountable for the Corona Virus Disease of 2019 (COVID-19), which was first spotted on Wuhan, China in December 2019 [1–3]. On March 11, 2020, this disease was acknowledged by the World Health Organization (WHO) as a global pandemic that has plagued almost all countries, accounting up to 770 million confirmed cases thus far and over 6.9 million deaths from all around the world as of August 27, 2023 [4]. MERS-CoV, short for Middle East Respiratory Syndrome Coronavirus, is also a *Betacoronavirus*, which was firstly identified in September of 2012 in Saudi Arabia [5]. Since then, more than 900 deaths have been reported due to the infection, meaning an approximate 35 % of lethality [6,7]. Hepatitis C virus (HCV) is another enveloped virus that is the main cause of viral chronic hepatitis worldwide, attributing to 58 million chronical infections and 300 thousands of deaths each year [8]. Progressive liver disease due to chronic infection, such as cirrhosis, steatosis, fibrosis and hepatocellular carcinoma could be developed for people infected with HCV, with the chances varying between 60 and 80 % [9].

Some measures that protect against the spread of SARS-CoV-2 are the use of masks or filters, in order to immobilize a high amount, but not 100 %, of the infectious droplets [10,11]. UV irradiation is also included in the methods that can inactivate the virus [12]. Silver nanoparticles were shown to have an antiviral effect against SARS-CoV-2, but they are considered toxic for the environment and quite costly [13]. To

* Corresponding author.
** Corresponding author.
E-mail addresses: anne.goffard@univ-lille.fr (A. Goffard), christophe.volkringer@centralelille.fr (C. Volkringer).

https://doi.org/10.1016/j.mtbio.2024.101165
Received 29 April 2024; Received in revised form 6 July 2024; Accepted 27 July 2024
Available online 2 August 2024

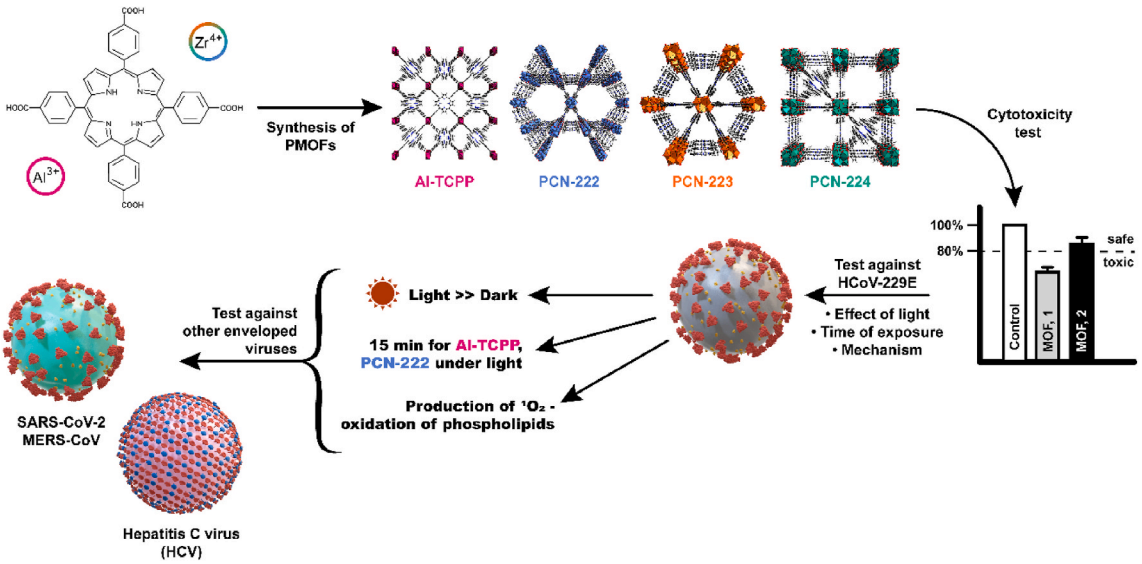

Fig. 1. Graphical scheme of the four PMOFs tested against four enveloped viruses, HCoV-229E, SARS-CoV-2, MERS-CoV and hepatitis C virus (HCV). The purple structure refers to Al-TCPP, the blue to PCN-222(Zr), the orange to PCN-223(Zr) and the green to PCN-224(Zr). The porphyrin ligand TCPP is displayed in the middle among the four PMOFs. (For interpretation of the references to color in this figure legend, the reader is referred to the Web version of this article.)

decontaminate both coronaviruses, quaternary ammonium salts can be used as disinfectants, such as benzalkonium chloride, but they could pose a threat to human health [14–17].

Metal-Organic Frameworks (MOFs) belongs to a class of crystalline porous solids having a hybrid nature, comprising of organic linkers that connect different combinations of inorganic metals or clusters. The high surface area they possess and the easy tunability of the chemical and structural proteins, renders them appealing for gas storage [18,19], catalysis [20–22], separation [23], drug delivery [24–30] or cancer therapy [27,31–33]. Porphyrin-based Metal-Organic Frameworks, sometimes referred to as porphyrinic Metal-Organic Frameworks (PMOFs) are a subcategory of MOFs, where the metal clusters are coordinated by macromolecular heterocyclic compounds, such as porphyrins that are formed by a tetrapyrrole ring [34,35]. These porphyrin ligands can generate reactive oxygen species (ROS) under visible light irradiation, such as hydroxyl radical (HO•), superoxide anion radical (O_2^-•) and singlet oxygen ($^1O_2$) [34].

These PMOFs could be ideal candidates for surface-modifications or functionalization of filters and/or textiles, that could be used as tools to impede the spread of serious to lethal diseases [36,37]. So far, MOFs have been successfully functionalized onto fabrics to create nanofiber filters for indoor air quality control and porous filters for environmental purposes [38,39]. Also, in one study, ZIF-8 was embedded in face masks as a catalyst to inactivate HCoV-OC43, a low pathogenic coronavirus, by 100 % after 1 h of UV irradiation [40]. Al-TCPP, a PMOF, has been grafted onto polypropylene textile by atomic layer deposition for the oxidation of organosulfur under light irradiation, paving the way on the functionalization of fibers with PMOFs [41].

For this study, four PMOFs, Al-TCPP, PCN-222 (or MOF-545), PCN-223 and PCN-224, all formed with the tetrakis(4-carboxyphenyl) porphyrin (TCPP) ligand, were selected and evaluated for the first time for their antiviral activity against HCoV-229E, SARS-CoV-2, MERS-CoV, and hepatitis C virus (HCV).

The phosphorylation of unsaturated phospholipids from the viral envelope due to singlet oxygen from ROS is a proven mechanism, that alters its fluidity and has an impact on its infectivity [42–45]. Therefore, the cytotoxicity of the selected PMOFs was assessed for four different concentrations by the Neutral Red method, against Huh7 TMPRSS2 and Vero81.6 cells. The highest non-cytotoxic concentration for each PMOF was used to proceed with the infection tests against the three coronaviruses, performing experiments both under dark and under visible light irradiation. In Fig. 1, a schematic approach of the encounter of PMOFs against the three coronaviruses and HCV is presented.

2. Methods and materials

2.1. Materials

Zirconium(IV) chloride ($ZrCl_4$, >99.5 %) and benzoic acid (99 %) were bought from Alfa Aesar. Aluminum(III) chloride hexahydrate ($AlCl_3$. $6H_2O$, >99.0 %) and formic acid were purchased from Honeywell Fluka. 5,10,15,20-(tetra-4-carboxyphenyl)porphyrin (TCPP, >98 %) was purchased from PorphyChem. Propionic acid (>99.5 %) was bought from Sigma-Aldrich. Acetone was bought from VWR. N–N-dimethylformamide (DMF, >99.9 %) was bought from Carlo Erba. Dulbecco's phosphate buffered saline (DPBS or PBS) 1×, Dulbecco's Modified Eagle Medium (DMEM) 1×, Trypsin-EDTA 0.05× were bought from Gibco. Fetal Bovine Serum (FBS) was bought from Eurobio. Neutral Red (NR) was bought from Clin-tech. Renilla Lysis buffer and the Luciferase reagent were bought from Promega.

Huh7, VeroE6 and Vero81 (ATCC number CCL-81) were grown in DMEM with 10 % FBS in an incubator at 37 °C with 5 % CO_2. Vero81 cells were subcloned (Vero81.6) to obtain a better overall infection rate [46]. HCoV-229E strain VR-740 (ATCC) and recombinant HCoV-229E-Luc (kind gift of V. Thiel) were used [47]. SARS-CoV-2 (isolate SARS-CoV-2/human/FRA/Lille_Vero-81-TMPRSS2/2020; NCBI MW575140) was propagated on Vero81 TMPRSS2 cells. MERS-CoV was recovered by transfecting the infectious clone of MERS-CoV-EMC12 in Huh-7 cells [48]. A cell culture-adapted strain (JFH1-CSN6A4) of HCV was produced as described previously [49].

2.2. Synthesis and characterization of PMOFs

The synthesis of the four pure and well crystallized PMOFs were based on modified protocols already reported in literature and detailed in supplementary information [50–54]. SEM images of the four PMOFs are shown in supplementary information, as well as PXRD patterns and TGA thermographs.

2.3. Cell culture and cytotoxicity assay

The four PMOFs were evaluated for their cytotoxicity with the

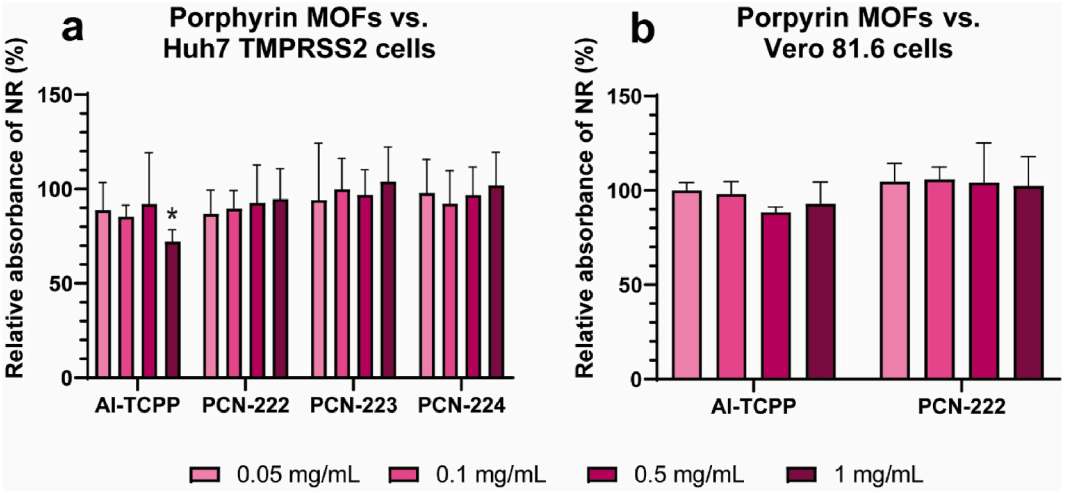

Fig. 2. Results from the three cytotoxicity experiments for the PMOFs that were studied in four different concentrations versus (a) Huh7 TMPRSS2 cells and (b) Vero81.6 cells. Relative absorbance of NR (%) is calculated by the ratio between the measurement of the absorbance of each MOF divided by the absorbance of the control. * For $p \leq 0.05$, as obtained after the statistical analysis with two-way ANOVA method (analysis of variance).

Neutral Red method (NR) against Huh7 TMPRSS2 and Vero81.6 cells, in order to proceed with the infection tests of the four viruses, that are done in presence of the respective cells. The preparation of the different concentrations of the materials, the protocol of the assay and the cell culture were done as in a previous study [55].

2.4. Infection tests with HCoV-229E, SARS-CoV-2, MERS-CoV and HCV

The protocol used for all of the infection tests was based in a previous study [55], where each material in its highest non-cytotoxic concentration is used and immersed in a tube containing the appropriate viral solution for a certain amount of time. Then, the tube was centrifuged and the supernatant with the virus was collected and added to the wells of a 96-well plate that contained cells. Therefore, the materials do not come in contact with the cells. The evaluation of the antiviral activity of the four materials was done by already known methods (luciferase activity, $TCID_{50}$, immunofluorescence, Western blot) for HCoV-229E, SARS-CoV-2 and hepatitis C virus (HCV) and tested both under light irradiation and under dark [55]. For MERS-CoV, a similar procedure as SARS-CoV-2 was followed and explained thoroughly in supporting information. Singlet oxygen $^1O_2$ characterization was done as presented in a previous study, with the use of sodium azide (NaN_3), that acts as a scavenger of $^1O_2$ [56]. Immunofluorescence characterization of the localization of structural proteins of HCV was followed as in previous studies, by using specific fluorescent antibodies, in order to determine the efficiency of the antiviral effect [9,57].

3. Results and discussion

3.1. Evaluation of cytotoxicity of PMOFs

The PMOFs Al-TCPP, PCN-222, PCN-223 and PCN-224 were studied for their cytotoxicity against Huh7 TMPRSS2 and Vero81.6 cells for the first time. After carrying out each cytotoxicity test three times for both cell lines, the graphs (Fig. 2) were plotted for each MOF with the four different concentrations (0.05, 0.1, 0.5 and 1 mg/mL), where the mean value of the three experiments and their standard deviations at a confidence level of 95 % are shown. The Neutral Red assay was used to evaluate their cytotoxicity, as it is considered the optimal one according to a previous study, whose absorbance is measured and is linked directly to the cytotoxicity in a linear fashion [55].

Regarding the cytotoxicity of PMOFs versus Huh7 TMPRSS2 cells, Al-TCPP shows toxicity at 1 mg/mL, and there is also a statistically significant difference between this value (72.1 % ± 6.4 %) and the control (100 %). The three structures of Zr-TCPP PMOF (PCN-222, PCN-223 and PCN-224) demonstrate no cytotoxicity up to 1 mg/mL, having values of 94.7 % ± 16.2 %, 103.9 % ± 18.2 % and 101.9 % ± 17.6 % respectively. Concerning Al-TCPP and PCN-222 against Vero81.6 cells, no signs of cytotoxicity up to 1 mg/mL were found. Therefore, the highest non-cytotoxic concentration against each cell line for each PMOF and their corresponding values are presented in Table 1. Hence, for the infection tests with HCoV-229E, MERS-CoV and HCV, 0.5 mg/mL of Al-TCPP were used. Concerning PCN-222, PCN-223 and PCN-224, 1 mg/mL was used for the tests against the four viruses.

Table 1
A summary of the highest non-cytotoxic concentration of each PMOF for each cell line, as calculated by the NR assay.

Metal-Organic Framework	Cell line	Highest Non-cytotoxic Concentration	Relative absorbance expressed in $\bar{x}$ (%) ± s (%)
Al-TCPP	Huh7	0.5 mg/mL	91.9 ± 27.2
	TMPRSS2	1 mg/mL	92.8 ± 11.7
	Vero81.6		
PCN-222	Huh7	1 mg/mL	94.7 ± 16.2
	TMPRSS2		102.4 ± 15.6
	Vero81.6		
PCN-223	Huh7	1 mg/mL	103.9 ± 18.2
	TMPRSS2		
PCN-224	Huh7	1 mg/mL	101.9 ± 17.6
	TMPRSS2		

3.2. Antiviral activity of PMOFs against HCoV-229E

In order to evaluate the antiviral activity of these four PMOFs, preliminary experiments took place against HCoV-229E-Luc, a luciferase recombinant virus of HCoV-229E, in Huh7 TMPRSS2 cells. A study of the kinetics of inactivation was performed at four different time points, 0, 5, 15 and 60 min, both under light exposure to the BSC's lamp (biosafety cabinet, fluorescent tube, 36 W, 3350 lumens, white light) and under dark, by wrapping the tubes with aluminum foil. Three experiments were carried out for each allotted time and the mean values are plotted in the graph found in Fig. 3a. The non-linear regression curves were calculated for each PMOF in GraphPad Prism 9, either under dark or light.

Under dark, Al-TCPP, PCN-223, and PCN-224 show a one-phase decay, and reach a plateau after 15 min of exposure, showing a

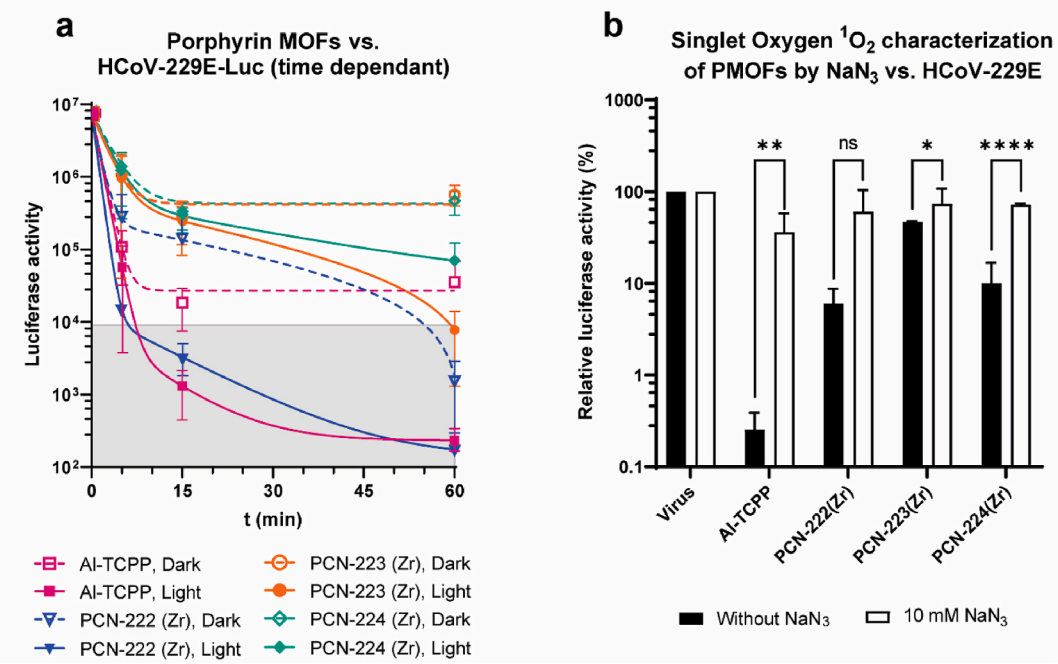

Fig. 3. Results from the infection tests of PMOFs against (a) HCoV-229E-Luc as a function of the time of contact between the PMOF and the virus, under dark (dotted line) and light exposure (solid line), highlighting the virucidal area (grey rectangle) (b) results from the infection tests of PMOFs and HCoV-229E-Luc in the absence or presence of 10 mM NaN_3 under light irradiation for 15 min. The means and standard deviations of the relative luciferase activity (%) of each PMOF are shown and expressed by dividing the absolute value of the material by the absolute value of the virus (negative control). Experiments were performed three times. Statistical analysis was performed by executing the Welch's *t*-test and p values were extracted. ns = not significant, * = $p \leq 0.05$, ** = $p \leq 0.01$ and **** = $p \leq 0.0001$.

substantial antiviral activity of 99.76 % (2.62 log_{10}), 96.46 % (1.45 log_{10}) and 95.84 % (1.38 log_{10}), respectively. The rest of the conditions exhibited a two-phase decay. The materials that decrease the infectivity by more than 99.9 % (>3 log_{10}) and therefore possess a virucidal activity against HCoV-229E-Luc are Al-TCPP and PCN-222 under light exposure of 15 min, showing an efficacy of 99.98 % (3.70 log_{10}) and 99.96 % (3.40 log_{10}) respectively. Notably, PCN-222 kept in dark seems to be virucidal after 60 min.

At 60 min of time of contact between the PMOFs and the virus, the effect of light exposure against dark is greater, augmenting its antiviral capacity, as it can be seen by the values between Al-TCPP (99.54 % or 2.34 log_{10} dark, 99.997 % or 4.52 log_{10} light), PCN-222 (99.98 % or 3.70 log_{10} dark, 99.998 % or 4.70 log_{10} light), PCN-223 (92.63 % or 1.13 log_{10} dark, 99.89 % or 2.95 log_{10} light) and PCN-224 (92.78 % or 1.14

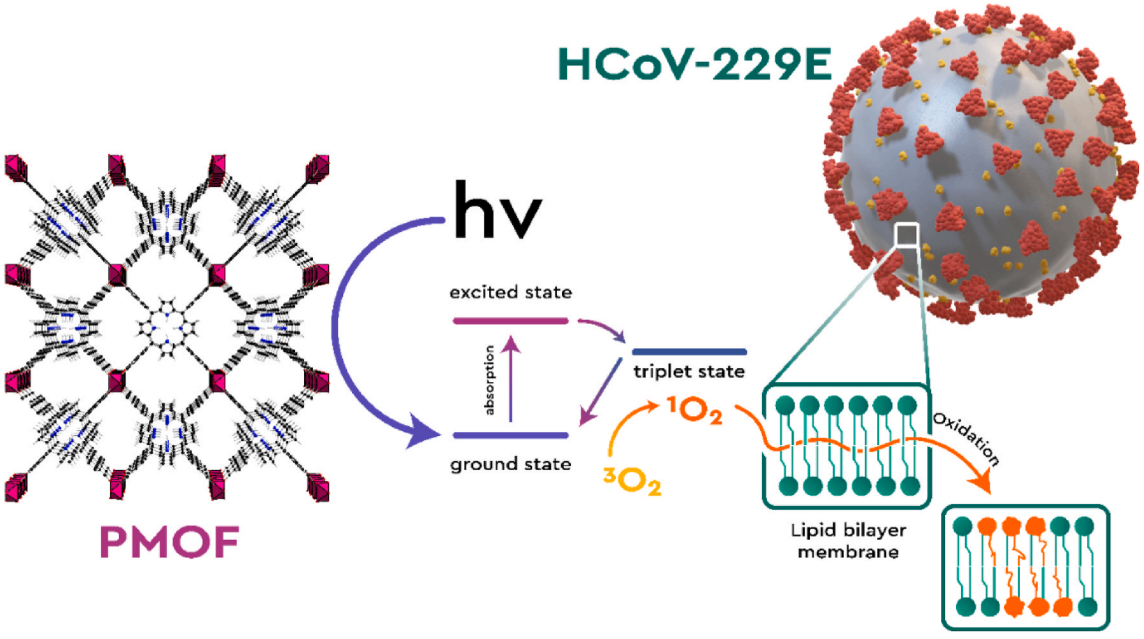

Fig. 4. Graphical scheme of the proposed mechanism of porphyrin-based MOFs (PMOFs) against coronaviruses. $^3O_2$ and $^1O_2$ refer to triplet and singlet oxygen respectively, while hv refers to the visible light that is irradiated and absorbed by the porphyrin ligand TCPP. The phospholipids of the lipid bilayer membrane (envelope) of the virus are presented in green (before oxidation) and in orange (after oxidation). (For interpretation of the references to color in this figure legend, the reader is referred to the Web version of this article.)

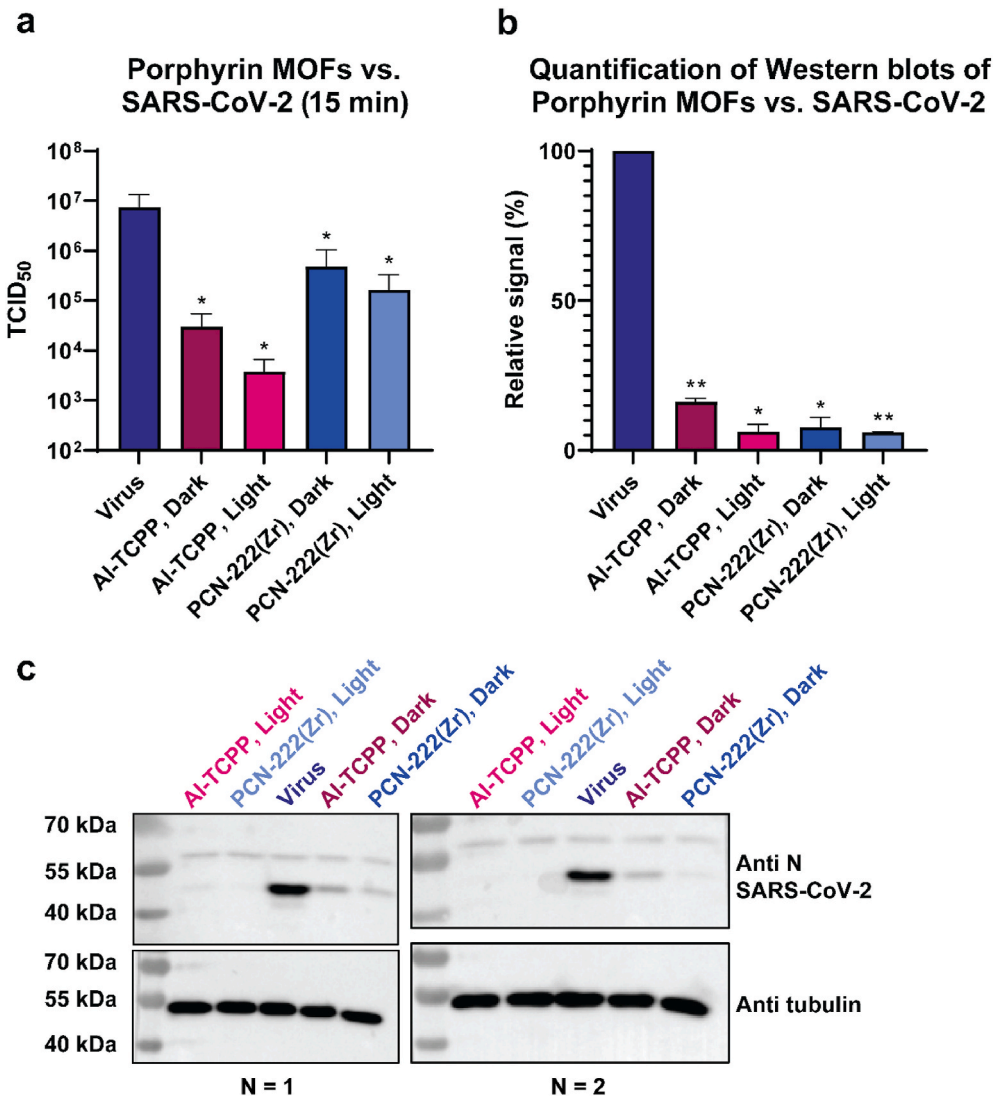

Fig. 5. Results from the infection tests of PMOFs and (a) SARS-CoV-2 under dark and light exposure of the materials during 15 min. (b) Quantification of the anti-N SARS-CoV-2 band for each material through the western blots. (c) Western blots of the two PMOFs tested under light and under dark. Anti-tubulin serves as a cell viability marker, while anti-N SARS-CoV-2 as a marker of the intracellular replication. Statistical analysis was performed by executing the Welch's *t*-test and p values were extracted. * = $p \leq 0.05$ and **** = $p \leq 0.0001$.

$\log_{10}$ dark, 99.1 % or 2.05 $\log_{10}$ light).

In order to explain the different efficacies of the four PMOFs and the main mechanism that is responsible for the inactivation of the virus, singlet oxygen $^1O_2$ characterization was performed by adding sodium azide (NaN_3) to the viral solution prior to the addition of the PMOFs. The time of contact between the PMOF and the virus was kept at 15 min NaN_3, serves as a specific quencher of the singlet oxygen, so it can be used to scavenge the $^1O_2$ produced from the excitation of the TCPP ligand under visible light [58]. Therefore, with NaN_3 being present with the virus and the PMOF, a decrease on their antiviral activity is to be expected. Indeed, a dramatic decrease of the efficiency of Al-TCPP (under light) and PCN-222 (under light) was demonstrated, from 99.75 % (2.60 $\log_{10}$) to 64.1 % (0.44 $\log_{10}$) and from 94.05 % (1.23 $\log_{10}$) to 40.31 % (0.22 $\log_{10}$) for each PMOF, respectively (Fig. 3b). From the three structures of Zr-TCPP (PCN-222, PCN-223 and PCN-224), the production of singlet oxygen $^1O_2$ is greater from PCN-222, then PCN-224 and lastly PCN-223 under 15 min of light irradiation, having similar results as found in literature [44]. Although, Al-TCPP seems to be more potent than the three structures of Zr-TCPP regarding the production of $^1O_2$ (Al-TCPP > PCN-222 > PCN-224 > PCN-223). A possible explanation, as also discussed by Liu et al.,[44]is the number of TCPP ligands linked per Zr- or Al-cluster, their distance between two neighbor molecules, as well as the pore size, meaning that larger pores facilitate the diffusion of light and $^1O_2$.

To conclude, Al-TCPP and PCN-222 showed a potent virucidal activity against HCoV-229E-Luc when exposed under light, under the short amount of time of 15 min of contact between the material and the virus, safely inactivating it by 99.96–99.98 %. The mechanism lies on the production of singlet oxygen $^1O_2$ from the porphyrin ligand, TCPP, that attacks the membrane of the virus, thus having an impact on it by prohibiting its entry to the cells (Fig. 4) [45].

3.3. *Antiviral activity of PMOFs against SARS-CoV-2, MERS-CoV and HCV*

Al-TCPP and PCN-222, which demonstrated the strongest antiviral effect against HCoV-229E-Luc, were evaluated for their efficacy against SARS-CoV-2, MERS-CoV, and hepatitis C virus (HCV). For the former, 1 mg/mL of Al-TCPP and PCN-222 was utilized, while for the other two 0.5 mg/mL of Al-TCPP were used, since the tests were done in Vero81.6 and Huh7 TMPRSS2 cells. Three experiments were carried out for each virus test and the antiviral activity of the PMOFs was calculated by the

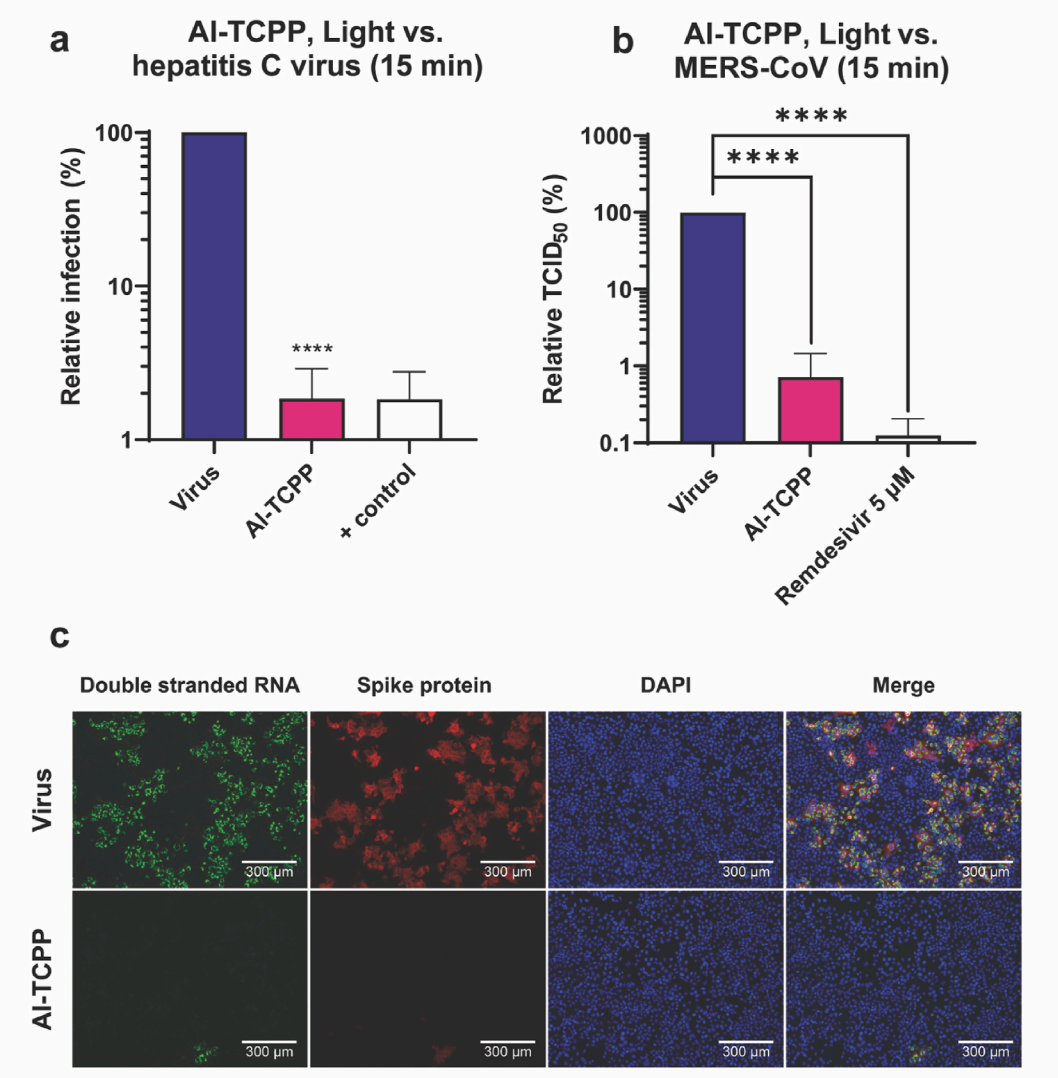

Fig. 6. Results from the infection tests of Al-TCPP versus (a) hepatitis C virus (HCV) and (b) MERS-CoV under light exposure of the material during 15 min. The mean value of three experiments and their respective standard deviations are shown. The virus control (negative control) serves as the 100 % of infection, while the positive (+) control represents the signal from the cells that did not get infected. (c) Representative images of immunofluorescence staining of co-localization of the double stranded RNA (green) and spike protein (red) of MERS-CoV in Huh7-AP cells before (Virus) and after the contact of the virus with Al-TCPP. 4,6-Diamidino-2-phenylindole (DAPI) staining serves as a marker of cell viability and thus the cytotoxicity of the PMOF. Statistical analysis was performed by executing the Welch's *t*-test and p values were extracted. **** = $p \leq 0.0001$. (For interpretation of the references to color in this figure legend, the reader is referred to the Web version of this article.)

determination of $TCID_{50}$ (Fig. 5a and b). For SARS-CoV-2, experiments under dark and light exposure during 15 min were done, while for MERS-CoV and HCV only the light condition was examined. Remdesivir (5 μM) was used as the positive control for MERS-CoV, since it is known that it has prophylactic and therapeutic properties, while for HCV the positive control was cells that did not get infected with the virus [59].

Regarding the results obtained for SARS-CoV-2 from the $TCID_{50}$ method (Fig. 5a), Al-TCPP shows a virucidal effect under 15 min of light exposure against the coronavirus, decreasing its infectivity by 99.95 % (3.30 log_{10}), while under dark it shows an antiviral inactivation of 99.6 % (2.40 log_{10}). PCN-222 has an antiviral activity of 93.48 % (1.19 log_{10}) and 97.80 % (1.66 log_{10}) under dark and light, respectively, which are statistically significant with respect to the negative control, although these reductions in titer are not meaningful from a virucidal point of view. These results seem to be in accordance with the tests done with HCoV-229E, where Al-TCPP showed a better efficacy than PCN-222. Also, the biochemistry of each virus is different, meaning that the molecules that construct the viral envelope and the viral proteins have an analogous morphology, but not the exact same composition of amino-acids; therefore it could explain why there are differences in the activity of these PMOFs [60–62]. Western blots for the detection of the viral protein N, that can confirm the intracellular replication of the virus, were done and the bands were quantified with the software ImageJ (Fig. 5b and c). In Fig. 6c, Al-TCPP and PCN-222(Zr) shows that under 15 min of light irradiation the viral entry is inhibited, hence the very low signal of the anti-N protein (6.14 % and 6.04 % respectively). Both materials seem to prevent the entry of SARS-CoV-2 under dark as well, but they display a smaller effect (16.16 % and 7.68 % respectively). The results obtained by this method validate the efficacy of the two PMOFs shown by the $TCID_{50}$ method. Taken all into account, Al-TCPP was selected as a possible candidate that could have a similar effect against HCV and MERS-CoV, this time testing it only under the best conditions: 15 min under light exposure.

The results obtained from the immunofluorescence HCV tests are displayed in Fig. 6a. Al-TCPP reduces its infectivity by 98.15 % (1.73 log_{10}), a value which is comparable to the one of the positive control (98.16 % or 1.74 log_{10}). Moreover, in the case of the MERS-CoV tests (Fig. 6b), Al-TCPP decreases the infectivity of the virus by 99.28 % (2.14

log_{10}), whose value is very similar to the one of the positive control (Remdesivir, 99.88 % or 2.92 log_{10}). Therefore, we consider that Al-TCPP shows potent antiviral activities for HCV and MERS-CoV, when exposed to light for as few as 15 min.

Immunofluorescence (IF) was used in order to validate and visualize the results obtained by the $TCID_{50}$ method for MERS-CoV. As seen in Fig. 6c, the staining with anti-double strand (green) and anti-S protein antibodies (red) depicts the co-localization of the double stranded RNA and spike protein of MERS-CoV, an indicator of the successful infection of the Huh7-AP cells. In blue (DAPI), the viability of the cells is shown, and on the right an image where the three different colored layers are merged. Two conditions were tested, without the addition of Al-TCPP to calculate the infection percentage of the virus control, and after the contact of 15 min with the PMOF, under light. As seen, less cells are infected after the addition of Al-TCPP, due to the phospholipid oxidation from the singlet oxygen produced from the TCPP ligand, as proved before. No signs of cytotoxicity were observed between the control and the Al-TCPP condition. Therefore, the IF images verify the results obtained by the $TCID_{50}$ method.

All taken together, Al-TCPP shows an incredible antiviral effect within 15 min of visible light irradiation against SARS-CoV-2, HCV and MERS-CoV. PCN-222(Zr) shows a lesser effect against SARS-CoV-2, compared to the one with HCoV-229E. Of note, the mechanism of inactivation of the two coronaviruses and HCV is the same as HCoV-229E, where $^1O_2$ is produced through the excitation of the porphyrin ligand by visible light and the envelope of the viruses are impaired, thus affecting the entry mechanism of them in the cells [45].

4. Conclusions

To summarize, four porphyrin-based Metal-Organic Frameworks (PMOFs) were assessed for their antiviral activity against three coronaviruses for the first time. At first, their effect on cell viability was evaluated with the Neutral Red assay, which was previously reported to be the ideal method of evaluating the cytotoxicity. Al-TCPP was found to be toxic at 1 mg/mL for Huh7 TMPRSS2 cells, but PCN-222, PCN-223 and PCN-224 showed no signs of cytotoxicity up to 1 mg/mL for the same cell line. For Vero81.6 cells, Al-TCPP and PCN-222 could be used up to 1 mg/mL without any significant cytotoxicity. In 15 min, Al-TCPP demonstrated the best virucidal activity against four viruses, HCoV-229E, SARS-CoV-2, MERS-CoV and HCV. From the three Zr-TCPP structures tested, PCN-222 was found to be the best performing one.

The mechanism of action against the viruses was studied by the use of sodium azide, a scavenger of $^1O_2$, and proven that it lies on the production of singlet oxygen, that comes from the excitation of the porphyrin ligand (TCPP) under visible light, which can attack the lipid bilayer membrane (envelope) of the virus. This indirect mechanism is ideal for functionalizing the PMOF onto textiles, like for the case of Al-TCPP on polypropylene, so as to hinder the infectivity of these viruses [41]. A future perspective for these materials would be to produce PMOF-composites for real-life applications, and to shape them as membrane, granulates, fabrics or masks. Also, studies on their stability under air and humidity should take place, along with leaching tests prior to their applications.

Funding sources

This work was partially supported by the PEARL program (Program for Early-stage Researchers in Lille).

CRediT authorship contribution statement

Orfeas-Evangelos Plastiras: Writing – review & editing, Writing – original draft, Methodology, Investigation, Data curation. **Peggy Bouquet:** Investigation, Formal analysis. **Imelda Raczkiewicz:** Writing – review & editing, Investigation. **Sandrine Belouzard:** Investigation, Validation. **Esther Martin De Fourchambault:** Writing – review & editing, Investigation. **Jeremy Dhainaut:** Writing – review & editing. **Jean-Philippe Dacquin:** Writing – review & editing. **Anne Goffard:** Writing – review & editing, Writing – original draft, Supervision, Investigation, Funding acquisition. **Christophe Volkringer:** Writing – review & editing, Writing – original draft, Supervision, Project administration, Funding acquisition.

Declaration of competing interest

The authors declare that they have no known competing financial interests or personal relationships that could have appeared to influence the work reported in this paper.

Data availability

Data will be made available on request.

Acknowledgments

The authors would like to thank Laurence Burylo and Philippe Devaux for their assistances with the synthesis and XRD powder patterns measurements (UCCS). The “Fonds Européen de Développement Régional (FEDER)", “CNRS”, “Région Hauts de France” and “Ministère de l’Education Nationale de l’Enseignement Supérieur et de la Recherche” are acknowledged for the funding of X-ray diffractometers and Scanning electron Microscopes from the Chevreul Institute platform. O.-E. Plastiras thanks I-SITE ULNE for the fund from the program PEARL (Program for Early-stage Researchers in Lille), financed by the Marie Skłodowska-Curie Actions, from the H2020 program of the European Commission (Agreement N° 847569).

Appendix A. Supplementary data

Supplementary data to this article can be found online at https://doi.org/10.1016/j.mtbio.2024.101165.

References

[1] J. Zheng, SARS-CoV-2: an emerging coronavirus that causes a global threat, Int. J. Biol. Sci. 16 (10) (2020) 1678–1685, https://doi.org/10.7150/ijbs.45053.
[2] D.L. McKee, A. Sternberg, U. Stange, S. Laufer, C. Naujokat, Candidate drugs against SARS-CoV-2 and COVID-19, Pharmacol. Res. 157 (2020), https://doi.org/10.1016/j.phrs.2020.104859.
[3] H.H. Wang, X.M. Li, T. Li, S.B. Zhang, L.Z. Wang, X. Wu, J.Q. Liu, The genetic sequence, origin, and diagnosis of SARS-CoV-2, Eur. J. Clin. Microbiol. Infect. Dis. 39 (9) (2020) 1629–1635, https://doi.org/10.1007/s10096-020-03899-4.
[4] World Health Organization (WHO), Coronavirus disease 2019 (COVID-19) situation report 158. https://www.who.int/publications/m/item/weekly-epidemiological-update-on-covid-19—1-september-2023. (Accessed 3 September 2024).
[5] B. Guery, J. Poissy, L. el Mansouf, C. Sejourne, N. Ettahar, X. Lemaire, F. Vuotto, A. Goffard, S. Behillil, V. Enouf, et al., Clinical features and viral diagnosis of two cases of infection with Middle East Respiratory Syndrome coronavirus: a report of nosocomial transmission, Lancet 381 (9885) (2013) 2265–2272, https://doi.org/10.1016/s0140-6736(13)60982-4.
[6] World Health Organization (WHO), Middle East respiratory syndrome coronavirus (MERS-CoV). https://www.who.int/news-room/fact-sheets/detail/middle-east-respiratory-syndrome-coronavirus-(mers-cov) (Accessed 30 October 2024).
[7] World Health Organization (WHO), Middle East respiratory syndrome coronavirus (MERS-CoV) - Saudi Arabia. https://www.who.int/emergencies/disease-outbreak-news/item/2023-DON484. (Accessed 21 January 2024).
[8] World Health Organization (WHO). Hepatitis C. https://www.who.int/news-room/fact-sheets/detail/hepatitis-c (accessed 30 October 2023).
[9] E.M. de Fourchambault, N. Callens, J.M. Saliou, M. Fourcot, O. Delos, N. Barois, Q. Thorel, S. Ramirez, J. Bukh, L. Cocquerel, et al., Hepatitis C virus alters the morphology and function of peroxisomes, Front. Microbiol. 14 (2023), https://doi.org/10.3389/fmicb.2023.1254728.
[10] A.C. Morris, K. Sharrocks, R. Bousfield, L. Kermack, M. Maes, E. Higginson, S. Forrest, J. Pereira-Dias, C. Cormie, T. Old, et al., The removal of airborne severe Acute respiratory syndrome coronavirus 2 (SARS-CoV-2) and other microbial bioaerosols by air filtration on coronavirus disease 2019 (COVID-19) surge units, Clin. Infect. Dis. 75 (1) (2022) E97–E101, https://doi.org/10.1093/cid/ciab933.

[11] Y. Nazarenko, Air filtration and SARS-CoV-2, Epidemiology and Health 42 (2020), https://doi.org/10.4178/epih.e2020049.
[12] N. Ruetalo, S. Berger, J. Niessner, M. Schindler, Inactivation of aerosolized SARS-CoV-2 by 254 nm UV-C irradiation, Indoor Air 32 (9) (2022), https://doi.org/10.1111/ina.13115.
[13] S.S. Jeremiah, K. Miyakawa, T. Morita, Y. Yamaoka, A. Ryo, Potent antiviral effect of silver nanoparticles on SARS-CoV-2, Biochem. Biophys. Res. Commun. 533 (1) (2020) 195–200, https://doi.org/10.1016/j.bbrc.2020.09.018.
[14] A.L. Frantz, Chronic quaternary ammonium compound exposure during the COVID-19 pandemic and the impact on human health, Toxicology and Environmental Health Sciences 15 (3) (2023) 199–206, https://doi.org/10.1007/s13530-023-00173-w.
[15] B.H. Ogilvie, A. Solis-Leal, J.B. Lopez, B.D. Poole, R.A. Robison, B.K. Berges, Alcohol-free hand sanitizer and other quaternary ammonium disinfectants quickly and effectively inactivate SARS-CoV-2, J. Hosp. Infect. 108 (2021) 142–145, https://doi.org/10.1016/j.jhin.2020.11.023.
[16] G.S. Selwyn, C.Y. Ye, S.B. Bradfute, Anti-SARS-CoV-2 activity of surgical masks infused with quaternary ammonium salts, Viruses-Basel 13 (6) (2021), https://doi.org/10.3390/v13060960.
[17] M.K. Ijaz, R.W. Nims, S.S. Zhou, K. Whitehead, V. Srinivasan, T. Kapes, S. Fanuel, J. H. Epstein, P. Daszak, J.R. Rubino, et al., Microbicidal actives with virucidal efficacy against SARS-CoV-2 and other beta- and alpha-coronaviruses and implications for future emerging coronaviruses and other enveloped viruses, Sci. Rep. 11 (1) (2021), https://doi.org/10.1038/s41598-021-84842-1.
[18] J. Dhainaut, M. Bonneau, R. Ueoka, K. Kanamori, S. Furukawa, Formulation of metal-organic framework inks for the 3D printing of robust microporous solids toward high-pressure gas storage and separation, ACS Appl. Mater. Interfaces 12 (9) (2020) 10983–10992, https://doi.org/10.1021/acsami.9b22257.
[19] M. Leloire, J. Dhainaut, P. Devaux, O. Leroy, H. Desjonqueres, S. Poirier, P. Nerisson, L. Cantrel, S. Royer, T. Loiseau, et al., Stability and radioactive gaseous iodine-131 retention capacity of binderless UiO-66-NH2 granules under severe nuclear accidental conditions, J. Hazard Mater. 416 (2021), https://doi.org/10.1016/j.jhazmat.2021.125890.
[20] N.D. McNamara, G.T. Neumann, E.T. Masko, J.A. Urban, J.C. Hicks, Catalytic performance and stability of (V) MIL-47 and (Ti) MIL-125 in the oxidative desulfurization of heterocyclic aromatic sulfur compounds, J. Catal. 305 (2013) 217–226, https://doi.org/10.1016/j.jcat.2013.05.021.
[21] K. Shen, X.D. Chen, J.Y. Chen, Y.W. Li, Development of MOF-derived carbon-based nanomaterials for efficient catalysis, ACS Catal. 6 (9) (2016) 5887–5903, https://doi.org/10.1021/acscatal.6b01222.
[22] W.Y. Zhao, T. Ding, Y.T. Wang, M.Q. Wu, W.F. Jin, Y. Tian, X.G. Li, Decorating Ag/AgCl on UiO-66-NH2: synergy between Ag plasmons and heterostructure for the realization of efficient visible light photocatalysis, Chin. J. Catal. 40 (8) (2019) 1187–1197, https://doi.org/10.1016/s1872-2067(19)63377-2.
[23] N. Manousi, O.E. Plastiras, N.P. Kalogiouri, C.K. Zacharis, G.A. Zachariadis, Metal-organic frameworks in bioanalysis: extraction of small organic molecules, Separations 8 (5) (2021), https://doi.org/10.3390/separations8050060.
[24] C.D. Ding, L. Tong, J. Feng, J.J. Fu, Recent advances in stimuli-responsive release function drug delivery systems for tumor treatment, Molecules 21 (12) (2016), https://doi.org/10.3390/molecules21121715.
[25] P. Horcajada, C. Serre, G. Maurin, N.A. Ramsahye, F. Balas, M. Vallet-Regi, M. Sebban, F. Taulelle, G. Ferey, Flexible porous metal-organic frameworks for a controlled drug delivery, J. Am. Chem. Soc. 130 (21) (2008) 6774–6780, https://doi.org/10.1021/ja710973k.
[26] B.M. Jarai, Z. Stillman, L. Attia, G.E. Decker, E.D. Bloch, C.A. Fromen, Evaluating UiO-66 metal-organic framework nanoparticles as acid-sensitive carriers for pulmonary drug delivery applications, ACS Appl. Mater. Interfaces 12 (35) (2020) 38989–39004, https://doi.org/10.1021/acsami.0c10900.
[27] S. Mallakpour, E. Nikkhoo, C.M. Hussain, Application of MOF materials as drug delivery systems for cancer therapy and dermal treatment, Coord. Chem. Rev. 451 (2022), https://doi.org/10.1016/j.ccr.2021.214262.
[28] B. Maranescu, A. Visa, Applications of metal-organic frameworks as drug delivery systems, Int. J. Mol. Sci. 23 (8) (2022), https://doi.org/10.3390/ijms23084458.
[29] C.Y. Sun, C. Qin, X.L. Wang, Z.M. Su, Metal-organic frameworks as potential drug delivery systems, Expet Opin. Drug Discov. 10 (1) (2013) 89–101, https://doi.org/10.1517/17425247.2013.741583.
[30] Y. Wang, J.H. Yan, N.C. Wen, H.J. Xiong, S.D. Cai, Q.Y. He, Y.Q. Hu, D.M. Peng, Z. B. Liu, Y.F. Liu, Metal-organic frameworks for stimuli-responsive drug delivery, Biomaterials 230 (2020), https://doi.org/10.1016/j.biomaterials.2019.119619.
[31] C.C. Chu, M. Su, J. Zhu, D.S. Li, H.W. Cheng, X.Y. Chen, G. Liu, Metal-organic framework nanoparticle-based biomineralization: a new strategy toward cancer treatment, Theranostics 9 (11) (2019) 3134–3149, https://doi.org/10.7150/thno.33539.
[32] N.Y. Chun, S.N. Kim, Y.S. Choi, Y.B. Choy, PCN-223 as a drug carrier for potential treatment of colorectal cancer, J. Ind. Eng. Chem. 84 (2020) 290–296, https://doi.org/10.1016/j.jiec.2020.01.010.
[33] W. Zhang, Y.B. Ma, Y.A. Li, H.P. Wang, A low cytotoxic porous zinc-adeninate metal-organic framework carrier: pH-triggered drug release and anti-breast cancer study, J. Iran. Chem. Soc. 16 (1) (2019) 65–71, https://doi.org/10.1007/s13738-018-1481-1.
[34] J.J. Chen, Y.F. Zhu, S. Kaskel, Porphyrin-based metal-organic frameworks for biomedical applications, Angew. Chem. Int. Ed. 60 (10) (2021) 5010–5035, https://doi.org/10.1002/anie.201909880.
[35] X. Zhang, M.C. Wasson, M. Shayan, E.K. Berdichevsky, J. Ricardo-Noordberg, Z. Singh, E.K. Papazyan, A.J. Castro, P. Marino, Z. Ajoyan, et al., A historical perspective on porphyrin-based metal-organic frameworks and their applications, Coord. Chem. Rev. 429 (2021), https://doi.org/10.1016/j.ccr.2020.213615.
[36] N. Couzon, M. Ferreira, S. Duval, A. El-Achari, C. Campagne, T. Loiseau, C. Volkringer, Microwave-assisted synthesis of porous composites MOF-textile for the protection against chemical and nuclear hazards, ACS Appl. Mater. Interfaces 14 (18) (2022) 21497–21508, https://doi.org/10.1021/acsami.2c0324721497.
[37] M.X. Chen, Q. Hu, X.Y. Wang, W. Zhang, A review on recent trends of the antibacterial nonwovens air filter materials: classification, fabrication, and application, Sep. Purif. Technol. 330 (2024), https://doi.org/10.1016/j.seppur.2023.125404.
[38] Y. Bian, R. Wang, S. Wang, C. Yao, W. Ren, C. Chen, L. Zhang, Metal–organic framework-based nanofiber filters for effective indoor air quality control, J. Mater. Chem. A 6 (32) (2018) 15807–15814, https://doi.org/10.1039/c8ta04539a.
[39] H. Xiao, Z.X. Low, D.B. Gore, R. Kumar, M. Asadnia, Z.X. Zhong, Porous metal-organic framework-based filters: synthesis methods and applications for environmental remediation, Chem. Eng. J. 430 (2022), https://doi.org/10.1016/j.cej.2021.133160.
[40] D. Givirovskaia, G. Givirovskiy, M. Haapakoski, S. Hokkanen, V. Ruuskanen, S. Salo, V. Marjomaki, J. Ahola, E. Repo, Modification of face masks with zeolite imidazolate framework-8: a tool for hindering the spread of COVID-19 infection, Microporous Mesoporous Mater. 334 (2022), https://doi.org/10.1016/j.micromeso.2022.111760.
[41] D.T. Lee, J.D. Jamir, G.W. Peterson, G.N. Parsons, Protective fabrics: metal-organic framework textiles for rapid photocatalytic sulfur mustard simulant detoxification, Matter 2 (2) (2020) 404–415, https://doi.org/10.1016/j.matt.2019.11.005.
[42] Z. Zhou, T. Wang, T.T. Hu, C.H. Cheng, S.L. Yu, H. Li, S.Y. Liu, L.F. Ma, M.T. Zhao, R.Z. Liang, et al., Facile synthesis of 2D Al-TCPP MOF nanosheets for efficient sonodynamic cancer therapy, Mater. Chem. Front. 7 (8) (2023) 1684–1693, https://doi.org/10.1039/d2qm01333a.
[43] Y.Y. Liu, A.J. Howarth, J.T. Hupp, O.K. Farha, Selective photooxidation of a mustard-gas simulant catalyzed by a porphyrinic metal-organic framework, Angew. Chem. Int. Ed. 54 (31) (2015) 9001–9005, https://doi.org/10.1002/anie.201503741.
[44] Y.Y. Liu, L.J. Chen, X. Zhao, X.P. Yan, Effect of topology on photodynamic sterilization of porphyrinic metal-organic frameworks, Chem.–Eur. J. 27 (39) (2021) 10151–10159, https://doi.org/10.1002/chem.202100920.
[45] F. Vigant, J. Lee, A. Hollmann, L.B. Tanner, Z.A. Ataman, T. Yun, G.H. Shui, H. C. Aguilar, D. Zhang, D. Meriwether, et al., A mechanistic paradigm for broad-spectrum antivirals that target virus-cell fusion, PLoS Pathog. 9 (4) (2013), https://doi.org/10.1371/journal.ppat.1003297.
[46] L. Desmarets, N. Callens, E. Hoffmann, A. Danneels, M. Lavie, C. Couturier, J. Dubuisson, S. Belouzard, Y. Rouille, A reporter cell line for the automated quantification of SARS-CoV-2 infection in living cells, Front. Microbiol. 13 (2022), https://doi.org/10.3389/fmicb.2022.1031204.
[47] S.H.E. van den Worm, K.K. Eriksson, J.C. Zevenhoven, F. Weber, R. Zust, T. Kuri, R. Dijkman, G.H. Chang, S.G. Siddell, E.J. Snijder, et al., Reverse genetics of SARS-related coronavirus using vaccinia virus-based recombination, PLoS One 7 (3) (2012), https://doi.org/10.1371/journal.pone.0032857.
[48] F. Almazán, M.L. DeDiego, I. Sola, S. Zuñiga, J.L. Nieto-Torres, S. Marquez-Jurado, G. Andrés, L. Enjuanes, Engineering a replication-competent, propagation-defective Middle East respiratory syndrome coronavirus as a vaccine candidate, mBio 4 (5) (2013), https://doi.org/10.1128/mBio.00650-13.
[49] L. Goueslain, K. Alsaleh, P. Horellou, P. Roingeard, V. Descamps, G. Duverlie, Y. Ciczora, C. Wychowski, J. Dubuisson, Y. Rouillé, Identification of GBF1 as a cellular factor required for hepatitis C virus RNA replication, J. Virol. 84 (2) (2010) 773–787, https://doi.org/10.1128/jvi.01190-09.
[50] D.W. Feng, Z.Y. Gu, Y.P. Chen, J. Park, Z.W. Wei, Y.J. Sun, M. Bosch, S. Yuan, H. C. Zhou, A highly stable porphyrinic zirconium metal-organic framework with shp-a topology, J. Am. Chem. Soc. 136 (51) (2014) 17714–17717, https://doi.org/10.1021/ja510525s.
[51] D.W. Feng, W.C. Chung, Z.W. Wei, Z.Y. Gu, H.L. Jiang, Y.P. Chen, D. J. Darensbourg, H.C. Zhou, Construction of ultrastable porphyrin Zr metal-organic frameworks through linker elimination, J. Am. Chem. Soc. 135 (45) (2013) 17105–17110, https://doi.org/10.1021/ja408084j.
[52] D.W. Feng, Z.Y. Gu, J.R. Li, H.L. Jiang, Z.W. Wei, H.C. Zhou, Zirconium-metalloporphyrin PCN-222: mesoporous metal-organic frameworks with ultrahigh stability as biomimetic catalysts, Angew. Chem. Int. Ed. 51 (41) (2012) 10307–10310, https://doi.org/10.1002/anie.201204475.
[53] J.R. Jin, Porphyrin-based metal-organic framework catalysts for photoreduction of CO2: understanding the effect of node connectivity and linker metalation on activity, New J. Chem. 44 (36) (2020) 15362–15368, https://doi.org/10.1039/d0nj03507f.
[54] A. Fateeva, P.A. Chater, C.P. Ireland, A.A. Tahir, Y.Z. Khimyak, P.V. Wiper, J. R. Darwent, M.J. Rosseinsky, A water-stable porphyrin-based metal-organic framework active for visible-light photocatalysis, Angew. Chem. Int. Ed. 51 (30) (2012) 7440–7444, https://doi.org/10.1002/anie.201202471.
[55] O.-E. Plastiras, P. Bouquet, C. Lecoeur, J. Dhainut, J.-P. Dacquin, S. Royer, T. Loiseau, A. Goffard, C. Volkringer, Cytotoxicity and effectiveness of archetypal metal-organic frameworks (HKUST-1, UiO-66, MIL-53, MIL-125) against coronaviruses (HCoV-229E and SARS-CoV-2), Microporous Mesoporous Mater. (2023), https://doi.org/10.1016/j.micromeso.2023.112975.
[56] T. Meunier, L. Desmarets, S. Bordage, M. Bamba, K. Hervouet, Y. Rouille, N. Francois, M. Decossas, V. Sencio, F. Trottein, et al., A photoactivable natural product with broad antiviral activity against enveloped viruses, including highly pathogenic coronaviruses, Antimicrob. Agents Chemother. 66 (2) (2022), https://doi.org/10.1128/aac.01581-21.

[57] Y. Rouillé, F. Helle, D. Delgrange, P. Roingeard, C. Voisset, E. Blanchard, S. Belouzard, J. McKeating, A.H. Patel, G. Maertens, et al., Subcellular localization of hepatitis C virus structural proteins in a cell culture system that efficiently replicates the virus, J. Virol. 80 (6) (2006) 2832–2841, https://doi.org/10.1128/jvi.80.6.2832-2841.2006.

[58] M. Bancirova, Sodium azide as a specific quencher of singlet oxygen during chemiluminescent detection by luminol and Cypridina luciferin analogues, Luminescence 26 (6) (2011) 685–688, https://doi.org/10.1002/bio.1296.

[59] J.J. Malin, I. Suarez, V. Priesner, G. Fatkenheuer, J. Rybniker, Remdesivir against COVID-19 and other viral diseases, Clin. Microbiol. Rev. 34 (1) (2021), https://doi.org/10.1128/cmr.00162-20.

[60] M.M. Medina-Enriquez, S. Lopez-Leon, J.A. Carlos-Escalante, Z. Aponte-Torres, A. Cuapio, T. Wegman-Ostrosky, ACE2: the molecular doorway to SARS-CoV-2, Cell Biosci. 10 (1) (2020), https://doi.org/10.1186/s13578-020-00519-8.

[61] F. Scialo, A. Daniele, F. Amato, L. Pastore, M.G. Matera, M. Cazzola, G. Castaldo, A. Bianco, ACE2: the major cell entry receptor for SARS-CoV-2, Lung 198 (6) (2020) 867–877, https://doi.org/10.1007/s00408-020-00408-4.

[62] A.R. Fehr, S. Perlman, Coronaviruses: an overview of their replication and pathogenesis, Coronaviruses: Methods and Protocols 1282 (2015) 1–23, https://doi.org/10.1007/978-1-4939-2438-7_1.